

Linewise kinetic Monte Carlo study of silicon dislocation dynamicsS. Scarle,* C. P. Ewels,[†] M. I. Heggie, and N. Martsinovich
CPES, University of Sussex, Falmer, Brighton, BN1 9QJ, United Kingdom

(Received 6 March 2003; revised manuscript received 9 September 2003; published 20 February 2004)

We present a number of n -fold way kinetic Monte Carlo simulations of the glide motion of 90° partial dislocations in silicon. We undertake a survey of ratios of kink formation energy F_k to kink migration barrier W_m , over a range of temperatures and applied stresses. These simulations are compared with Hirth-Lothe theory and an extension to the Hirth-Lothe theory of Kawata and Ishiota. The latter is found to give the best description of the system. Using literature first principle values for the kink and soliton formation and migration energies, a model combining both strained bond and soliton mediated motion shows a negligible contribution to dislocation motion from the solitons. The high soliton pair creation barrier was limiting and a soliton mediated mechanism for dislocation motion would have to achieve thermal equilibrium concentration via impurity or point defect interaction to be effective. We also show that if this can be overcome solitons greatly increase the mobility of the dislocation, even without a binding energy between solitons and kinks. The simulation coded here is easily expandable to incorporate further dislocation line effects such as impurities at the line.

DOI: 10.1103/PhysRevB.69.075209

PACS number(s): 61.72.Hh, 61.72.Bb, 61.72.Lk

I. INTRODUCTION

The strength of ductile materials is determined by dislocation motion on the densest packed crystal slip planes. Silicon is often taken as a model system for high lattice friction (covalent and ceramic) solids, but there is still debate over the structure and movement of dislocations even in this simple diamond structure solid.

The problem of dislocations in semiconductors is now within the powers of modern hybrid computing techniques. These use static first principle calculations of significant processes (e.g., kink formation/migration) to parametrize larger scale simulations, i.e., kinetic Monte Carlo simulations of dislocation motion.

The general study of dislocations in silicon is of renewed importance, as wafer sizes grow larger and strained-layer structures are needed. The primary dislocations in silicon are the 60° mixed and screw dislocations. These each dissociate respectively into 90° and 30° partials and two 30° partials, separated by a stacking fault of approximately 50 \AA when in equilibrium.¹ A dislocation line is considered to move forward not in a single spontaneous step but instead at various points along the line (kinks) which then propagate the forward motion along the line. These forward steps involve atomic displacements, but their precise nature is still in doubt. Dislocation motion comes about from the thermally activated process of throwing forward line segments generating these kinks in pairs, sometimes called double kinks, which with the application of an external stress are forced apart, thus carrying the dislocation into the next Peierls valley. There is much evidence for the existence of such kinks from pulse deformation, internal friction,² weak-beam electron microscopy, and spectroscopy.^{3,4}

The first model proposed for silicon dislocation glide was a simple bond switching mechanism, called the bond rotation or Jones model.⁵ Here two silicon atoms within the dislocation core are rotated about their bond center, by around 90° about a $\langle 111 \rangle$ axis, and rebonded to the lattice. This both

initially forms a kink pair and with repeated application to neighboring sites, causes the kinks to migrate apart and eventually annihilate. This Jones model was first studied with interatomic potentials⁵ and subsequently with first principle calculations giving activation energies close to experimental values,^{6,7} with one exception.⁸

Note that if applied to every other reconstructed bond along the core of a single period reconstructed 90° partial core^{9,10} this bond switching converts the core to an alternative proposed double-period core structure.¹¹

More recently, an alternative mechanism invoking free radicals or solitons was found to give rise to similar energies,^{6,12,13} provided these solitons were in thermal equilibrium. Depending on its reconstruction a 90° partial core has two phases, usually labeled *right* and *left*, depending which way the reconstruction bonds are leaning. At phase interfaces, there are antiphase defects¹⁴ which we refer to here as solitons¹³ with a 1.4-eV formation energy. The soliton is an undercoordinated silicon atom, a free radical in chemical nomenclature, and hence highly reactive. The radical can migrate rapidly along the line, with a migration barrier of only 0.15 eV. The soliton model is a suggested additional atomic scale process for kinks within dislocation glide. The dangling bond of the soliton can catalyze kink formation, and therefore greatly reduces its energy barrier. The concept of solitons was first proposed by Hirsch under a different moniker;⁹ the nomenclature is not universal and other names such as *phase-switching defects*, *antiphase defects*, and *flips* have also been used.

In both the Jones and soliton model, dislocation motion is controlled by two primary parameters, the kink formation energy, F_k , and the kink migration energy W_m . In this work we present a number of n -fold way kinetic Monte Carlo simulations of dislocation motion dynamics, using a description of the dislocation line which allows the addition of further defects to the system (Sec. III). These give a broad survey of the phase space of kink formation energy F_k and kink migration barrier W_m , over a range of temperatures and stresses (Sec. IV A). We then compare this to the standard

theory in this field, that of Hirth and Lothe,¹⁵ and also to a suggested improvement to this theory by Kawata and Ishiota.¹⁶ Finally we examine the potential rôle of solitons (Sec. IV B).

II. BACKGROUND

Dislocations in silicon have been well studied since Shockley's first suggestion of their core structure some 50 years ago. In the last decade, there have been experimental measurements of dislocation mobilities of small segments in silicon films^{17,18} and high-resolution transmission electron microscopy of kink dynamics through the imaging of kinks on a partial dislocation in silicon,¹⁹ as well as *in situ* recording of motion.^{20,21} There have been many theoretical attempts to characterize and parametrize dislocation motion.^{5–8,13,22–25}

To give an overview of kink motion on glide dislocations in silicon: At low temperatures (420 °C) and under high stress, straight sided hexagonal loops of 60° and screw orientation form.²⁶ However, this is reliant on high temperature (~850 °C) predeformation to produce sufficient dislocation density, otherwise the silicon is brittle at 420 °C. Dislocation dissociation gives two partial loops, one enclosing the other and both bounding a stacking fault. Each loop has the same Burgers vector and as the orientation of the line changes, so the character of the partial changes between 30° and 90°. The absence of 60° dislocations is due to their high mobility, so as the circular loop expands, its 60° segments move quickest and vanish, leaving the slower segments. The 60° segment has a higher mobility since it consists of segments of 90° and 30° partials joined by kinks. Thus when it moves, no kinks need to be formed ($F_k=0$) and the activation energy just depends on W_m .

Note that the mobility of a partial dislocation to a small degree depends on whether it is leading or trailing, and on its type,²⁶ but these distinctions between 90° and 30° partials only give rise to variations in activation energy of less than 0.1 eV, which is comparable to local spin density approximation uncertainties, i.e., within the errors of the *ab initio* calculations described later. Hence we do not consider these effects in the calculations presented here, and feel justified in our choice of the 90° partial.

However, even if the 30° partials were dominant, we would therefore compare our calculated activation energies against the 60° perfect dislocation energy (2.2 eV), corrected for the 0.1-eV difference leads to 2.1 eV for the 90° partial, thus improving agreement with our calculated values.⁶

A. Hirth-Lothe theory

Hirth and Lothe (HL) theory¹⁵ assumes that the elementary processes of dislocation motion is kink pair formation followed by their diffusive glide along the dislocation line. The abrupt kink model invoked by HL finds dislocation glide velocity v_{dis} to be thermally activated in one of two possible regimes:

$$v_{dis} = v_0 d \exp\left(-\frac{F_k + W_m}{k_B T}\right)$$

or

$$v_{dis} = v_0 L \exp\left(-\frac{2F_k + W_m}{k_B T}\right), \quad (1)$$

where L is the segment length, d is the lattice period along the dislocation line, and

$$v_0 = \frac{2\nu_k \sigma b h^2}{k_B T}, \quad (2)$$

with ν_k the vibrational frequency of kinks (usually taken to be the silicon Debye frequency²⁷ $1.56 \times 10^{13} \text{ s}^{-1}$), σ is the resolved shear stress, b is the magnitude of the Burgers vector, and h is the distance between neighboring Peierls valleys (i.e., the *height* of a kink).

The effective activation energy E_A of the glide velocity is a linear combination of kink formation energy F_k and kink migration barrier W_m , and is determined by the applicable regime. $E_A = F_k + W_m$ for segments long enough so that kink lifetimes are limited by kink-kink annihilation, and $E_A = 2F_k + W_m$ for segments short enough for kink pairs to sweep out the whole segment. The characteristic length between these two regimes is twice the average kink separation obtained in thermal equilibrium

$$\lambda = d \exp\left(\frac{F_k}{k_B T}\right); \quad (3)$$

therefore, the steady state linear concentration of kinks becomes

$$\rho = \frac{2}{d} \exp\left(-\frac{F_k}{k_B T}\right). \quad (4)$$

Which of these two regimes is applicable to silicon, if indeed either of them, is still a matter of controversy.²⁸

B. Beyond Hirth-Lothe theory

Although it is a commonly used analysis of dislocation motion, the HL postulate of one unique kink mechanism is a huge simplification of the findings of atomistic simulations.^{7,25,29} Indeed, even under this approximation HL theory has shortcomings. Many suggest multiple core mechanisms operate simultaneously, with several distinct defect and kink species forming, moving, combining and annihilating. For example the work of Wang *et al.*³⁰ on the $a/2\langle 111 \rangle$ screw dislocation in tantalum has eight distinguishable single kink types leading to 16 types of kink pair.

An alternative, little referenced work of Kawata and Ishiota¹⁶ (KI) attempts to refine HL theory. They observe that HL makes three approximations, of which only the first is explicitly stated:

(1) Under small external stress, the concentration of kinks remains nearly the same as in thermal equilibrium.

(2) The correlation between kinks drifting under external stress may be ignored.

(3) The direct contribution of the processes of formation and annihilation of kink pairs to the whole movement of a dislocation may be neglected. The rôle of such processes

being restricted to an indirect contribution to maintain the kink density; i.e., the movement of the dislocation line is assumed to occur only by the migration of kinks.

These approximations are replaced in Kawata-Ishiota theory by the following four less restrictive approximations: (1) the line comprises of flat sections and single step kinks, (2) the fundamental changes to the system are single sections of the line being moved forward or backward by a single step (i.e., the creation/annihilation of a kink pair or the migration of a kink by a single repeat distance), (3) the rates of these moves only depend on neighboring sites ignoring longer range interactions, and (4) these rates are assumed to change linearly with applied stress.

This leads to the following form for the steady state kink concentration:

$$\rho = \frac{1}{d} \frac{2x}{1+2x} \quad \text{where} \quad x = \exp\left(-\frac{F_k}{k_B T}\right). \quad (5)$$

If this is then used in the rest of the HL formulation, ν_{dis} takes the form

$$\nu_{dis} = \nu_0 d \frac{\exp\left(-\frac{F_k + W_m}{k_B T}\right)}{1 + 2 \exp\left(-\frac{F_k}{k_B T}\right)}$$

or

$$\nu_{dis} = \nu_0 L \frac{\exp\left(-\frac{2F_k + W_m}{k_B T}\right)}{1 + 2 \exp\left(-\frac{F_k}{k_B T}\right)} \quad (6)$$

in the two different length regimes. (Note that the L -dependent behavior was not explicitly discussed in the original KI work), λ , the characteristic length between the regimes, becomes

$$\lambda = d \frac{1+2x}{x}. \quad (7)$$

C. Atomic scale processes

As mentioned above, there are two main suggestions for how kink motion in silicon moves the dislocation line. Firstly, the Jones or strained bond model, where kink formation and migration occur through successive application of a 90° rotation of a Si-Si bond in the glide plane about the bond center. Calculations of kink pair nucleation and expansion for this process give $E_A = 1.9$ eV with a small dependence on the kink pair width,⁵ assuming that the bond rotation is the rate limiting step.

The other model invokes solitons. Solitons are proposed as mediators for both kink formation and propagation,¹³ with an $E_A = 1.8$ eV, assuming that the formation energy of a kink pair at a soliton and the migration energy of a kink-soliton complex are the rate controlling processes. This is in addition to solitons being in thermal equilibrium.

Thus, E_A for both the strained bond and soliton mechanisms come close to the experimentally observed $E_A \approx 2.2$ eV for intrinsic silicon.¹⁸ We consider both mechanisms in our simulations. However, the main difference between the two mechanisms is that solitons, while being energetically expensive to create, once present lower the migration barrier of most kink species by around an order of magnitude (see soliton section).

III. MODEL

We take on board the idea of multi-scale modelling, since it is too computationally expensive to model an entire dislocation line system at an *ab initio* level. We use *ab initio* energy calculations for localized structures and then use these to parametrize a larger scale algorithmic model.

The larger scale evolution of the line is achieved via an n -fold way kinetic Monte Carlo (nkMC) approach.³¹⁻³⁵ Dislocation segments are assumed to lie in Peierls minima. The lattice has an effectively infinite extent in the direction of motion and is periodic perpendicular to it. The line moves due to the effects of thermal fluctuation and an applied stress. Kink-kink interactions beyond the first neighbor are neglected. The initial shape of the dislocation line in all cases is taken to be the perfectly straight single period reconstruction. As mentioned earlier, there is also a suggested double period reconstruction for the lowest energy state of the line. However, as the structure would be broken up as the line moves, our initial choice of starting state should not greatly affect the overall conclusions.

In the nkMC approach, all allowed events have a rate calculated for them. These can move the line either with or against the stress, since thermal fluctuations can overcome the additional energy bias caused by the stress. The rate for each event r_i is given by

$$r_i = \omega_0 \exp(-\Delta E_i / k_B T), \quad (8)$$

where i is the event number, ΔE_i the energy barrier of event i , and ω_0 the attempt frequency for which we use the silicon Debye frequency²⁷ $= 1.56 \times 10^{13}$ Hz. The sum of these rates is then used to determine the time till the next event, and the rates themselves act as probabilities.

Instead of trying random events at each time step and accepting or rejecting them based on a Boltzmann-like criterion, e.g., the Metropolis algorithm,³⁶ we choose and carry out an event m from all the possible events M at each step, such that

$$\frac{\sum_{i=0}^{m-1} r_i}{M} < \xi_1 < \frac{\sum_{i=0}^m r_i}{M}, \quad (9)$$

where ξ_1 is a random number in the range (0,1). The time increment dt for each Monte Carlo (MC) step is dynamic and stochastic, and given by

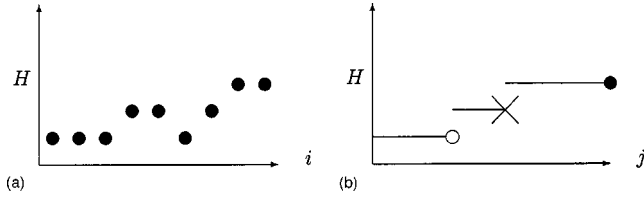


FIG. 1. Simplified plots to show the comparison between (a) point-wise and (b) line-wise; i being point along the line, j being section along the line. Symbols on plot (b) denote different hypothetical end structures along the line (e.g., kinks, solitons).

$$dt = -\frac{\ln \xi_2}{M} \sum_{i=0} r_i, \quad (10)$$

where ξ_2 is a second random number in the range (0,1). This formula for dt is rigorous,^{31–33,37} the work of Bulnes *et al.* gives a fuller description of the derivation of dt and the method in general.³³ This variable time step allows rates of greatly different magnitude to be included in the same model. In addition, since a move is carried out at every MC step, the long dead times that can be brought about by a fixed time step are removed.³⁷

In the standard method of describing a dislocation line to an MC simulation,^{37,38} the line is represented by a fixed number of sites. Each site i has a height H_i , giving the distance traveled from the original position by the dislocation line at that site under the stress. All sites can move either forward or back, which equates to the formation/annihilation or migration of kinks [Fig. 1(a)]. We call this the pointwise description.

“Linewise” is our more flexible description,^{39–41} and is similar to that of Cai *et al.* in that the line is described by a variable number of sections. Each section j is described by its length L_j and height H_j . However, we also state which defect structure the section ends, E_j , i.e., a positive or negative kink, soliton, etc. [Fig. 1(b)]. The L_j is measured in single period reconstruction bonds.

So long as the density of defects stays relatively low, longer dislocation lines can be considered more efficiently. This is because defect creation events for entire sections can be dealt with as a single event, as opposed to individually in pointwise. It is also easy to introduce further defects to the simulation; our model is coded so that properties of all line section ends are included via a parameter file.

At a high population of defect structures, the distinction between defects located *at* reconstructed bond sites along the dislocation core and those lying *between* them becomes more important. This is roughly equivalent to a change from inclusive to exclusive boundary conditions. Hence, in our simulation each end structure has an associated width. Kinks and other inter-reconstruction bond defects are of zero width, and must keep at least one reconstruction bond apart from other zero width defects. Defects that take up a reconstructed bond or bonds are of width one or more, and may abut other defects. Solitons, for example, are width one.

We shall now use the basic model of a step up kink (up-kink) and a step down kink (down-kink) to spell out how

TABLE I. Energy Barriers for moves in the Jones nkMC model.

Barrier	Move	Reasoning
W_m	kink migration	
$2F_k + W_m$	kink pair creation	creating two kinks plus moving them apart
W_m	kink pair annihilation	equivalent to kink migration

algorithmically moves are carried out: Kink migration involves changing the length of two neighboring sections so that $L_j \rightarrow L_j \pm 1$, while $L_{j+1} \rightarrow L_{j+1} \mp 1$. The creation of a positive kink pair involves replacing a previous section by three new sections. That is, a section of indeterminate length ending with an up-kink, followed by a unit length section ending in a down-kink and finally the remainder of the original section. The creation of a single defect can also take place in a similar manner.

The aforementioned computational saving comes from the following; as we discount long range interactions between defects all such pair creation events are equivalent along any given section and have equal rates. So, one can be randomly selected and used to represent all others for that section. The new combined rate being the original rate of one of these events multiplied by the length of the section. An equivalent algorithmic time saving is also made for the creation of single defects.

More complex moves are also possible, including the separation of a single defect into two, the merging of two defects into one, the transformation of one defect into another, and the transformation of two neighboring defects into a different pair. Note, that the line-wise formalism does not mean that the whole length of a given section of line moves simultaneously, only that their chance of movement can be considered together before choosing a single site to move.

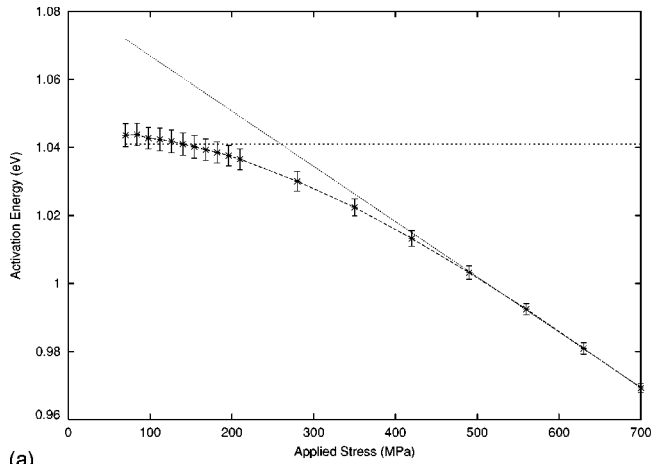
The aforementioned applied stress is implemented via a bias on the activation energies $\Delta E_i \rightarrow \Delta E_i \pm s$, depending on whether the line is being moved with or against the stress, where

$$s = \sigma b l h, \quad (11)$$

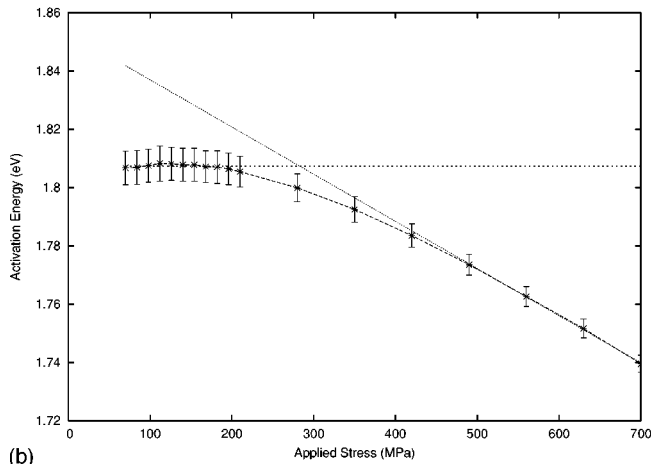
σ is the applied stress, b the magnitude of the Burgers vector of the dislocation, l the length of section of dislocation moving, namely the repeat distance along the dislocation line, and h the height change. This gives $s \approx 0.013$ eV for a stress of 70 MPa, in the case of a 90° partial in silicon.

TABLE II. F_k and W_m from Valladares *et al.* (Ref. 8), Öberg *et al.* (Ref. 6), and Nunes *et al.* (Ref. 7).

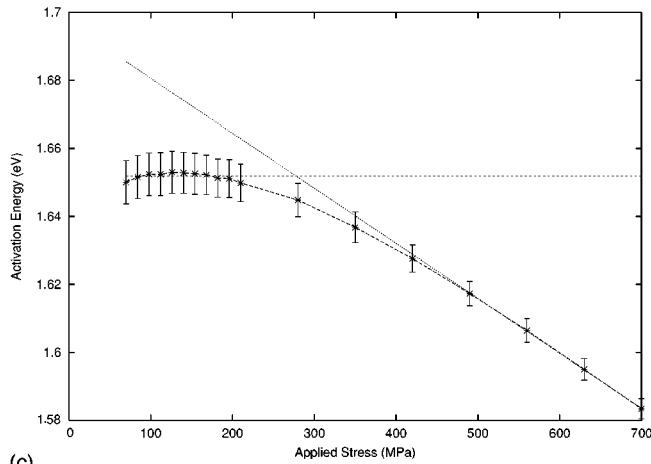
F_k /eV	W_m /eV	Reference
0.04	1.09	8
0.1	1.8	6
0.12	1.62	7



(a)



(b)



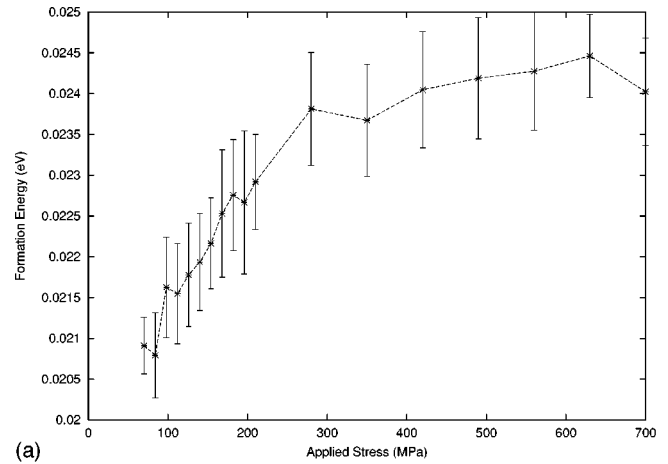
(c)

FIG. 2. Plots of effective E_A from nkMC runs with parameter sets derived from (a) Valladares *et al.* (Ref. 8), (b) Öberg *et al.* (Ref. 6), (c) Nunes *et al.* (Ref. 7). Data for lines can be found in Table IV.

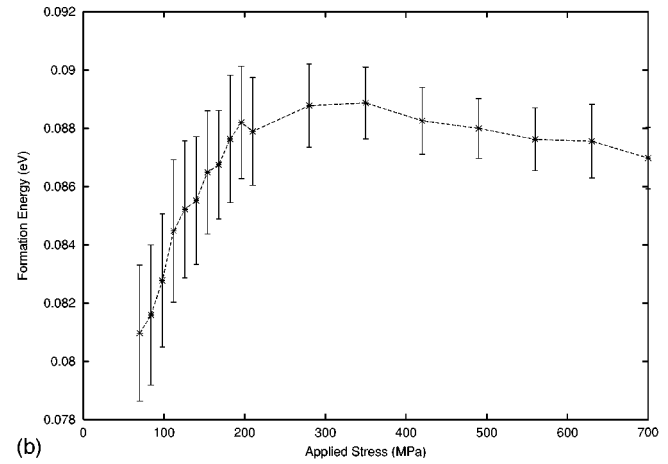
IV. RESULTS

A. Bond rotation model

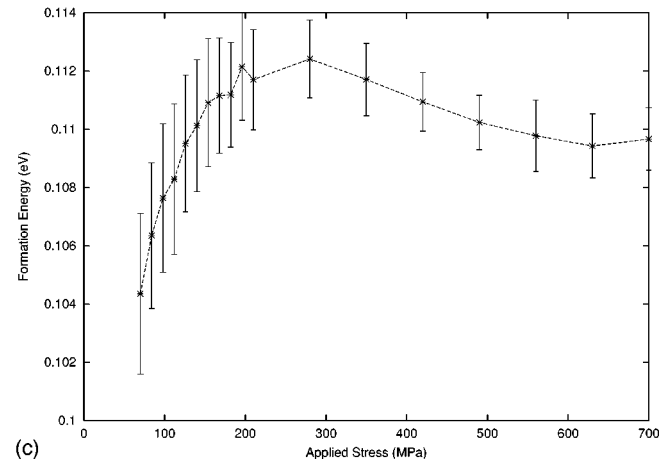
In our first simulation we have only two end structure defects, a kink either stepping up or down, both having a



(a)



(b)



(c)

FIG. 3. Plots of effective E_F from nkMC runs with parameter sets derived from (a) Valladares *et al.* (Ref. 8), (b) Öberg *et al.* (Ref. 6), (c) Nunes *et al.* (Ref. 7).

width of zero. This allows us to explore a dislocation operating using the Jones bond rotation model⁵ discussed earlier.

Many calculations have been carried out on this dislocation system in silicon, so we ran the same simulation with F_k and W_m from three pieces of work in the literature.⁶⁻⁸ The first uses a local density functional technique in a supercell, the second uses the same method but in a cluster, while the

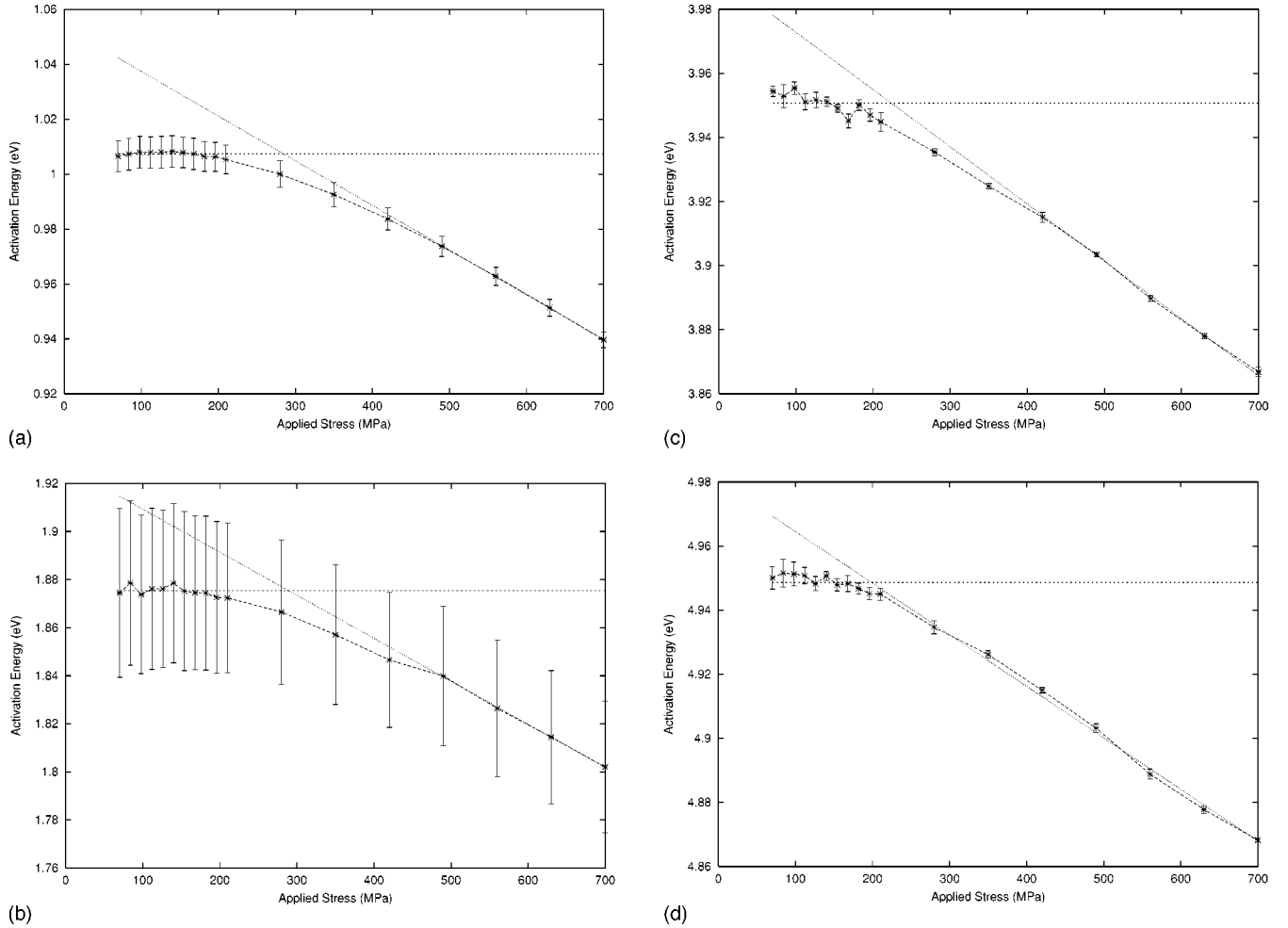


FIG. 4. Plots of effective E_A from nkMC runs with $W_m=1.0$ eV and (a) $F_k=0.1$ eV, (b) $F_k=0.5$ eV, (c) $F_k=1.5$ eV, (d) $F_k=2.0$ eV. Data for lines can be found in Table V.

final one uses a linear-scaling density matrix method. Table I lists their F_k and W_m values, all of these calculations follow the same broad trend $W_m \sim 1-2$ eV and F_k an order of magnitude lower. This leads to the barrier energies for our three basic moves in the simulation shown in Table II. The simulation for each pair of F_k and W_m , was run for ten million MC steps, for a 1000 site long line. The direction of motion was biased by a variable applied stress: from 70 MPa to 210 MPa, in steps of 7 MPa, then up to 700 MPa in steps of 70 MPa, at temperatures of between 500 and 1000 K, in steps of 100 K.

For each applied stress, best fits to Arrhenius plots of the velocity and the kink concentration were used to determine the effective activation barrier to dislocation glide E_A and the effective formation energy for kinks E_F . The effective activation energy being the activation energy apparent from an Arrhenius plot over our thermal range, while the effective formation energy being the energy which gives a thermal equilibrium concentration identical to our observed concentration. The results are shown in Figs. 2 and 3.

In general, it seems that at higher stresses $E_A \approx F_k + W_m - \alpha s$, with s being the stress in eV from Eq. (11). At lower stress this s dependence is lost and E_A saturates short of the

E_A at $s=0$, towards some constant value. Lines to indicate these two aspects have been added to the plots in Fig. 2. We can take the α to be the activation area of this dislocation system, the area of slip over which the shear stress works at the saddle point.

For a more complete investigation of the phase space of F_k and W_m , we then carried out simulations over the same ranges of temperature and stress with W_m set at 1.0 eV and F_k varied from 0.02 to 0.3 eV in steps of 0.02 eV and then up to 2.0 eV in steps of 0.1 eV. These showed the same behavior at low F_k but as F_k increases, we enter a second regime. Here, the high stress E_A becomes $2F_k + W_m - \alpha s$ while still saturating at low stresses (Fig. 4).

The crossover between $E_A \approx F_k + W_m - \alpha s$ and $E_A = 2F_k + W_m - \alpha s$ occurs at $F_k = 0.4-0.5$ eV. To understand this we must look back to KI theory and Eq. (7). When the characteristic length λ falls below the actual length of the system L , the system switches from $E_A = F_k + W_m$ to $E_A = 2F_k + W_m$. In cases of $F_k = 0.4-0.5$ eV, this cross over happens in the middle of our simulated temperature range of 500–1000 K, hence all the poorest fits for the Arrhenius plots are within this range (see Fig. 4). At higher or lower F_k , the crossover occurs outside of the 500–1000-K window. A plot of the

TABLE III. Energy Barriers for soliton moves in nkMC theory.

Barrier eV	Move	Reasoning
0.29	soliton-kink complex migration	W_m for soliton-kink complex
0.15	soliton migration	W_m for soliton
2.95	soliton pair creation	$2F_k + W_m$ create two solitons and move them apart
0.15	annihilation of soliton pair	equivalent to soliton migration
0.29	formation of kink-pair at a soliton produces a kink-soliton complex neighboring a kink	equivalent to soliton-kink complex migration
0.18	annihilation of a kink pair at a soliton	energy difference between soliton and kink-soliton complex (Ref. 12)

formation energy against these high stress E_A values extrapolated to zero stress ($s=0$) can be seen in Fig. 5, and this clearly shows the transition between the two regimes.

The activation energy plots tell us a number of things. At large stresses, there is an activation area equal to the smallest area of slip. As one would expect, it shows no correlation with F_k across our survey and on average ≈ 0.899 , if s is expressed in eV. Thus it roughly represents the energy due to the stress from a dislocation section of unit length in our system. This is the energy saving in the kink pair of critical width due to the work done by the applied stress over this width. This is an understandable difference between our simulations and KI and HL theories, and consonant with the Seeger-Schiller correction⁴² to HL theory at high stress when critical kink width is one site separation.

The fact that KI theory gives a much better description of our model than HL theory, can clearly be seen by the plots shown in Fig. 6. These show the percentage error between our simulations and either KI or HL theory for the concentration of kinks over a range of temperatures and stresses using Öberg *et al.*⁶ calculated values for F_k and W_m . The

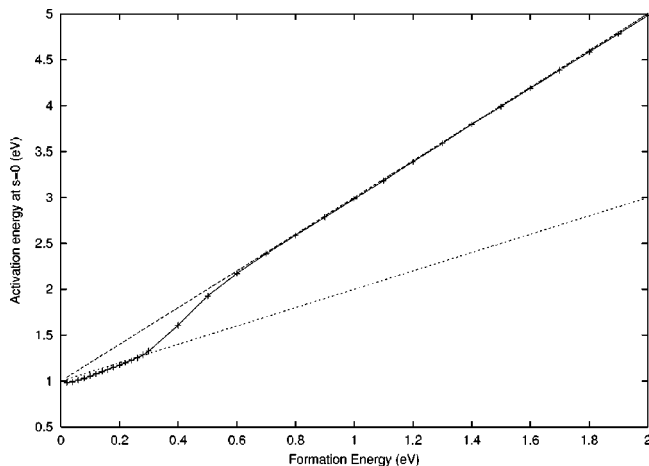


FIG. 5. The central line shows a plot of effective E_A extrapolated to zero stress ($s=0$) with $W_m=1$ eV, against formation energy F_k from the nkMC survey. The upper and lower lines show $2F_k + W_m$ and $F_k + W_m$, respectively.

errors for KI range from 0.45% to 28%, while those for HL range from 31% to 77%.

This plot of error in the kink concentration shows the deviation between our model and KI theory is at low temperature and high stresses. These deviations can be understood since our nkMC statistics will be worse at lower T , while at high stress the approximation of rates being proportional to stress made by KI becomes less appropriate.

From this it is clear that KI theory, is a better description of our model, and by inference we believe a better description of the actual physical system. Although at high stresses we achieve a linear plot for effective E_A , it clearly diverges from this linear behavior at lower stresses. The stress at the point of departure is inversely proportional to F_k . KI theory, with its linear stress dependence, has no way of describing this.

B. Solitons

We take the view that both strained bond and solitons can work together in our simulations. So, to add solitons we introduce three additional defect structures: soliton-kink step

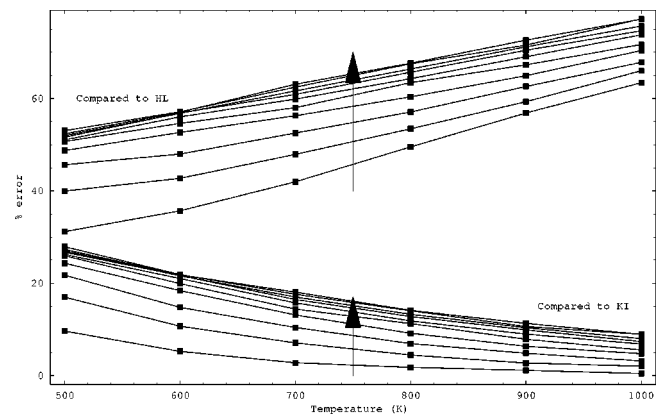


FIG. 6. Percentage error between the nkMC simulation using the Öberg *et al.* (Ref. 6) values and (a) KI and (b) HL for the linear concentration of kinks along the dislocation line. Each set of lines shows increasing stress from 70 MPa to 700 MPa, in steps of 70 MPa. Stress increases as we follow the arrows up each set.

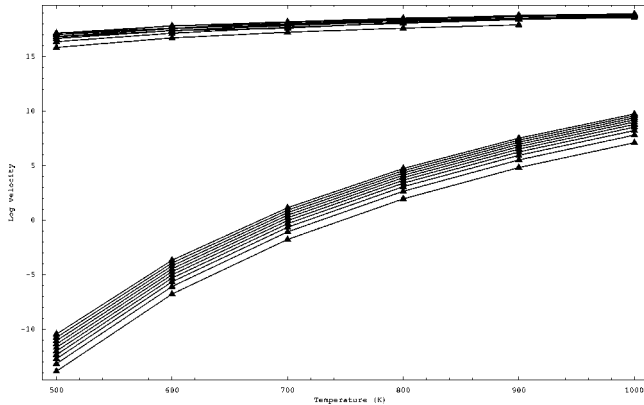


FIG. 7. Plot of natural log of velocity (sites per second) against temperature (K). The upper set are those with solitons included, while the lower are those without. Within each set stress increases as we go up the set from 70 MPa to 700 MPa, in steps of 70 MPa.

up complex, soliton-kink step down complex and the soliton itself. The complexes having width zero, while the soliton has width one.

We take further calculations¹² for parametrization, including the soliton migration barrier of 0.15 eV, and their kink pair nucleation barrier of 0.29 eV. We now add the moves as shown in Table III, taking the Öberg parameters as our base moves. As well as moves that allow kinks to move into/out of solitons and vice versa, producing/splitting kink-soliton complexes. We assume no binding energy between solitons and kinks, meaning that they can pass through each other. However, they can also move together as complexes. We also assume that two solitons migrating into each other will spontaneously annihilate.

Upon running the simulation with the same stress and temperature ranges as before, we saw a minimal change in the behavior of the system, almost within line thickness of plots shown. This is because although the F_k of a soliton is a thermally accessible 1.4 eV, we have to create them in pairs because of topological constraints. The time averaged concentrations of the solitons and kink-soliton complexes in these simulations are infinitesimal. They only appear fleetingly and then rapidly annihilate, being unable to maintain their thermal equilibrium concentration within the time frame of the simulation.

What is clear from our calculations is that some process is required to decrease the activation energy for formation of solitons, if they are to play an important role in the dislocation motion. However, we cannot discount solitons as a catalyst for dislocation motion, as they can offer more robust explanations of recombination enhanced glide^{43,44} and impurity pinning.⁴⁵ Additionally it may be possible to create singular solitons with a change of boundary conditions, (ours currently are periodic) or at some defect intersecting the dislocation line. Both of these may obviate the need to form solitons in pairs and hence potentially halve the activation energy for formation.

To investigate this we ran further simulations which were identical except that we started with a single soliton on the line (a concentration of 0.1% of sites) and removed the soli-

TABLE IV. E_A values for curves of Fig. 2, expressed in eV. s is also expressed in eV.

Source	E_A	E_A
	Constant section	Linear section
Ref. 8	1.041	$-0.867s + 1.08$
Ref. 6	1.807	$-0.863s + 1.85$
Ref. 7	1.652	$-0.862s + 1.70$

ton creation/annihilation moves. In this way, the soliton concentration was maintained above its equilibrium value.

A plot of these simulations can be seen in Fig. 7, and clearly shows increases in the final velocity of the dislocation line of many orders of magnitude. This shows that even without a binding energy between kinks and solitons, the brief contact between them and the catalytic effect of solitons on kink pair formation both greatly increase the dislocation mobility. However, to work this magic some other defect must assist and maintain the solitons at an increased concentration, for example in hydrogen enhanced dislocation glide (HEDG), where hydrogen may be able to lower the soliton pair formation energy by saturating one of the solitons. We are also currently examining the HEDG effect, where solitons may become more important, as hydrogen could lower the formation energy of a soliton pair by saturating one of the solitons.

V. CONCLUSIONS

In this study we have shown that the little known work of Kawata and Ishiota is more appropriate than Hirth-Lothe theory for dislocation dynamics, as it is better than Hirth-Lothe for describing the most basic set of moves to produce dislocation glide (see Table II). It still does not explain the stress dependence of the dislocation glide activation energy completely, as it does not include the necessary nonlinear stress terms. However, for a broad range of stress the approximation holds well, especially at higher temperature (see Fig. 4). Thus, for a closer agreement to modeled behavior we should use the Kawata-Ishiota forms for the kink concentration [Eq. (5)] in the two regimes. Further, we have shown that for solitons to affect the system, requires the influence of further defects and/or surface effects.

Now this code has been implemented it is a relatively trivial matter to model other dislocation-defect systems: All we require is the requisite formation and migration energies

TABLE V. E_A values for curves of Fig. 4 expressed in eV. s is also expressed in eV.

F_k	E_A	E_A
	Constant section	Linear section
0.1	1.007	$-0.867s + 1.05$
0.5	1.875	$-0.954s + 1.93$
1.5	3.951	$-0.952s + 3.99$
2.0	4.949	$-0.858s + 4.98$

as well as stress and temperature ranges, and we propose to acquire such data. We are now looking at simulating the HEDG process,¹⁸ by adding various hydrogenation moves and hydrogenated defect structures, as well as possible further work on defect line pinning.

ACKNOWLEDGMENT

We would like to thank the Sussex High Power Computing Initiative (SHPCI) for the use of the BFG computer resource.

-
- *Electronic address: s.scarle@umist.ac.uk. Current address: Chemistry Department, UMIST, Sackville Street, Manchester, M60 1QD, United Kingdom.
- †Current address: Departement Materiaux et Systems Composites, ONERA, DMSC, 29 Avenue de la Division Leclerc, 92322 Châtillon, France.
- ¹P.B. Hirsch, *Mater. Sci. Technol.* **1**, 666 (1985).
 - ²K. Maeda, M. Inoue, K. Suzuki, H. Amasuga, M. Nakamura, and E. Kanematsu, *J. Phys. III* **7**, 1451 (1997).
 - ³J.C.H. Spence, *Elec. Mic. Anal.* **153**, 23 (1997).
 - ⁴W. Benoit, G. Gremaud, and B. Queuet, *Mater. Sci. Eng., A* **164**, 42 (1993).
 - ⁵R. Jones, *Philos. Mag. B* **42**, 213 (1980).
 - ⁶S. Öberg, P.K. Sitch, R. Jones, and M.I. Heggie, *Phys. Rev. B* **51**, 13138 (1995).
 - ⁷R.W. Nunes, J. Bennetto, and D. Vanderbilt, *Phys. Rev. Lett.* **77**, 1516 (1996).
 - ⁸A. Valladares, J.A. White, and A.P. Sutton, *Phys. Rev. Lett.* **81**, 4903 (1998).
 - ⁹P.B. Hirsch, *J. Phys. (Paris), Colloq.* **40**, C6-27 (1979).
 - ¹⁰R. Jones, *J. Phys. (Paris), Colloq.* **40**, C6-33 (1979).
 - ¹¹R.W. Nunes, J. Bennetto, and D. Vanderbilt, *Phys. Rev. B* **57**, 10388 (1998).
 - ¹²C.P. Ewels, S. Leoni, M.I. Heggie, P. Jemmer, and E. Hernández, *Phys. Rev. Lett.* **84**, 690 (2000).
 - ¹³M.I. Heggie and R. Jones, *Philos. Mag. B* **48**, 365 (1983); **48**, 379 (1983).
 - ¹⁴P.B. Hirsch, *J. Phys. (Paris), Colloq.* **40**, C6-C117 (1979); *J. Microsc.* **118**, 3 (1980).
 - ¹⁵J. P. Hirth and J. Lothe, *Theory of Dislocations*, 2nd ed. (Krieger, Malabar, Florida, 1982).
 - ¹⁶Y. Kawata and S. Ishiota, *Philos. Mag. A* **48**, 921 (1983).
 - ¹⁷E.A. Stach, R. Hull, R.M. Tromp, M.C. Reuter, M. Copel, F.K. LeGoues, and J.C. Bean, *J. Appl. Phys.* **83**, 1931 (1998).
 - ¹⁸Y. Yamashita, F. Jyobe, Y. Kamiura, and K. Maeda, *Phys. Status Solidi A* **171**, 27 (1999); *Mater. Sci. Forum* **258-263**, 313 (1997).
 - ¹⁹H. Alexander, H.R. Kolar, and J.C.H. Spence, *Phys. Status Solidi A* **171**, 5 (1999).
 - ²⁰H. Kolar, J.C.H. Spence, and H. Alexander, *Phys. Rev. Lett.* **77**, 4031 (1996).
 - ²¹J.C.H. Spence, H.R. Kolar, and H. Alexander, *J. Phys. III* **7**, 2325 (1997).
 - ²²J.R.K. Bigger, D.A. McInnes, A.P. Sutton, M.C. Payne, I. Stich, R.P. King-Smith, D.M. Bird, and L.J. Clarke, *Phys. Rev. Lett.* **69**, 2224 (1992).
 - ²³Y.M. Huang, J.C.H. Spence, and O.F. Sankey, *Phys. Rev. Lett.* **74**, 3392 (1995).
 - ²⁴J. Bennetto, R.W. Nunes, and D. Vanderbilt, *Phys. Rev. Lett.* **79**, 245 (1997).
 - ²⁵V.V. Bulatov, S. Yip, and A.S. Argon, *Philos. Mag. A* **72**, 453 (1995).
 - ²⁶K. Wessel and H. Alexander, *Philos. Mag.* **35**, 1523 (1977).
 - ²⁷G. Dolling, in *Proceeding of Symposium on Inelastic Scattering of Neutrons in Solids and Liquids* (IAEA, Chalk River, 1963), Vol. II, 1963, pp. 37–38.
 - ²⁸Y. Yamashita, K. Maeda, K. Fujita, N. Usamai, K. Suzuki, S. Fukatsu, Y. Mera, and Y. Shiraki, *Philos. Mag. Lett.* **67**, 165 (1993).
 - ²⁹M.S. Duesbery, *Acta Metall.* **31**, 1747 (1983).
 - ³⁰G.F. Wang, A. Strachen, T. Cagin, and W.A. Goddard, *J. Comput. Aided Mater. Des.* **8**, 117 (2002).
 - ³¹A.B. Bortz, M.H. Kalos, and J.L. Lebowitz, *J. Comp. Physiol.* **17**, 10 (1975).
 - ³²G.N. Hassold and E.A. Holm, *Comput. Phys.* **7**, 97 (1993).
 - ³³F.M. Bulnes, V.D. Pereyra, and J.L. Riccardo, *Phys. Rev. E* **58**, 86 (1998).
 - ³⁴G.H. Gilmer, *J. Cryst. Growth* **35**, 15 (1976).
 - ³⁵P.A. Maksym, *Semicond. Sci. Technol.* **3**, 594 (1988).
 - ³⁶N. Metropolis, D.W. Rosenbluth, M.N. Rosenbluth, A.H. Teller, and E. Teller, *J. Chem. Phys.* **21**, 1087 (1953).
 - ³⁷C.C. Battaile, D.J. Srolovitz, and J.E. Butler, *J. Appl. Phys.* **82**, 6293 (1997).
 - ³⁸K. Lin and D.C. Chrzan, *Phys. Rev. B* **60**, 3799 (1999).
 - ³⁹W. Cai, V.V. Bulatov, J.F. Justo, A.S. Argon, and S. Yip, *Phys. Rev. Lett.* **84**, 3346 (2000); *Comput. Mater. Sci.* **23**, 124 (2002).
 - ⁴⁰W. Cai, V.V. Bulatov, and S. Yip, *J. Comput. Aided Mater. Des.* **6**, 175 (1999).
 - ⁴¹S. Scarle, N. Martsinovich, C.P. Ewels, and M.I. Heggie, *Physica B* **308-310**, 493 (2001).
 - ⁴²A. Seeger and P. Schiller, *Acta Metall.* **10**, 348 (1962).
 - ⁴³G. Vanderschaeve, C. Levade, and D. Caillard, *J. Phys.: Condens. Matter* **49**, 10093 (2000).
 - ⁴⁴M. Werner, E.R. Weber, M. Bartsch, and U. Messerschmidt, *Phys. Status Solidi A* **150**, 337 (1995).
 - ⁴⁵K. Sumino, *Phys. Status Solidi A* **171**, 111 (1999).